

See discussions, stats, and author profiles for this publication at: <https://www.researchgate.net/publication/354439395>

# A Monte–Carlo Study of Giant Vesicle Morphologies in Nonequilibrium Environments

Article in *Biophysical Journal* · September 2021

DOI: 10.1016/j.bpj.2021.09.005

CITATIONS

0

READS

34

6 authors, including:



**Mitja Drab**

University of Ljubljana

15 PUBLICATIONS 90 CITATIONS

SEE PROFILE



**Žiga Pandur**

University of Ljubljana

5 PUBLICATIONS 73 CITATIONS

SEE PROFILE



**Samo Penič**

University of Ljubljana

16 PUBLICATIONS 87 CITATIONS

SEE PROFILE

Some of the authors of this publication are also working on these related projects:



Piezoelectric Biomaterials for Electro-stimulated Regeneration [View project](#)



mathematical model of the hip [View project](#)

# A Monte Carlo study of giant vesicle morphologies in nonequilibrium environments

Mitja Drab,<sup>1,2,\*</sup> Žiga Pandur,<sup>3</sup> Samo Penič,<sup>4</sup> Aleš Iglič,<sup>1,2</sup> Veronika Kralj-Iglič,<sup>2,5</sup> and David Stopar<sup>3</sup>

<sup>1</sup>Laboratory of Physics, Faculty of Electrical Engineering, <sup>2</sup>Laboratory of Clinical Biophysics, Faculty of Medicine, <sup>3</sup>Department of Food Science and Technology, Biotechnical Faculty, <sup>4</sup>Laboratory of Bioelectromagnetics, Faculty of Electrical Engineering, and <sup>5</sup>Laboratory of Clinical Biophysics, Faculty of Health Sciences, University of Ljubljana, Ljubljana, Slovenia

**ABSTRACT** It is known that giant vesicles undergo dynamic morphological changes when exposed to a detergent. The solubilization process may take multiple pathways. In this work, we identify lipid vesicle shape dynamics before the solubilization of 1,2-dioleoyl-*sn*-glycero-3-phosphocholine giant vesicles with Triton X-100 (TR) detergent. The violent lipid vesicle dynamics was observed with laser confocal scanning microscopy and was qualitatively explained via a numerical simulation. A three-dimensional Monte Carlo scheme was constructed that emulated the nonequilibrium conditions at the beginning stages of solubilization, accounting for a gradual addition of TR detergent molecules into the lipid bilayers. We suggest that the main driving factor for morphology change in lipid vesicles is the associative tendency of the TR molecules, which induces spontaneous curvature of the detergent inclusions, an intrinsic consequence of their molecular shape. The majority of the observed lipid vesicle shapes in the experiments were found to correspond very well to the numerically calculated shapes in the phase space of possible solutions. The results give an insight into the early stages of lipid vesicle solubilization by amphiphilic molecules, which is nonequilibrium in nature and very difficult to study.

**SIGNIFICANCE** This study reports on dynamic morphology changes of 1,2-dioleoyl-*sn*-glycero-3-phosphocholine lipid vesicles in the presence of detergent Triton X-100 and presents a novel, to our knowledge, three-dimensional Monte Carlo scheme that offers insight into the observed shape changes based on molecular geometry of amphiphiles in nonequilibrium environments.

## INTRODUCTION

Lipid vesicles are soft spherical structures. Under nonequilibrium conditions, driven by the influx of materials and energy, fascinating vesicle dynamic behavior has been observed, such as 1) tumbling, in which a vesicle undergoes a periodic flipping motion; 2) trembling, in which vesicle shape fluctuates and the orientation oscillates in time; and 3) tank treading, in which an ellipsoid vesicle's major axis maintains a fixed orientation with respect to the flow direction while the membrane rotates about the vorticity axis (1). The transitions between these dynamical modes depend on shear rate, viscosity ratio between the inner and outer fluid viscosities, and reduced volume, which is a measure of a vesicle's asphericity (2). Different morphological patterns may emerge in gradual and rapid environmental changes

even between the identical initial and final equilibrium states.

In this work, we will show that extensive lipid vesicle reshaping can be induced with the addition of detergent molecules. The detergent reshaping of lipid vesicle can lead to vesiculation and solubilization (3,4). Previously, shape transformations with a varying degree of similarity were observed when vesicles were exposed to baths of oleic or fatty acids (5,6), but the mechanisms of dynamic changes were not considered.

Phospholipids self-assemble in a way that prevents exposure of their hydrophobic moieties to water (7). A lipid vesicle is composed of two flexible layers of phospholipids in which, in an aqueous solution, polar headgroups are oriented outward facing the solution and the hydrophobic tails of the two layers are facing each other. Two factors primarily govern whether a lipid will form a stable bilayer: solubility and molecular shape. For self-assembled structures such as bilayers, the lipid should have low solubility in water, which can be described as a low critical micelle concentration (8,9).

Submitted March 22, 2021, and accepted for publication September 2, 2021.

\*Correspondence: [mitja.drab@fe.uni-lj.si](mailto:mitja.drab@fe.uni-lj.si)

Editor: Rumiana Dimova.

<https://doi.org/10.1016/j.bpj.2021.09.005>

© 2021 Biophysical Society.

Above the critical micelle concentration, lipid molecules aggregate and form larger structures such as micelles, inverted micelles, or bilayers (10). The propensity for a lipid bilayer depends on shape of the lipid molecule (9,11–13). If a particular lipid monolayer structure has too large a deviation from zero spontaneous curvature, it will not form a lipid bilayer (14). Neglecting the anisotropy of the shape of lipid molecules (15,16), phospholipids such as phosphatidylethanolamine, phosphatic acid, diacylglycerol, and cardiolipin have a small polar headgroup/acyl chain ratio, which makes them roughly inverted conical in (dynamic) shape, which in turn imposes a negative monolayer curvature. Monolayers with these lipids bend in such a way that the headgroups come closer together and do not form lipid bilayers. Conversely, lipids with a large headgroup/acyl chain ratio, such as lysophosphatidylcholine or the large headgroups in phosphatidylinositol phosphates, that confers a conical shape to the lipids thereby favor the bending of the membrane into a positive curvature, bending the monolayer away from the headgroups (7,9,13). On the other hand, phosphatidylcholine and phosphatidylserine are cylindrical lipids that form a flat monolayer and consequently have a large propensity for lipid bilayers.

Introducing a conical or inverted-conical molecule into the lipid bilayer, such as a detergent, introduces stress. The partition coefficient that describes the detergent equilibrium between the bilayer and the aqueous solution is governed by the hydrophobicity of the detergent and its shape. The detergents are curvophilic, i.e., they have a tendency to form a positive spontaneous curvature (17). Curvophilic molecules are known to accumulate in the curved regions of bilayers, where the membrane inclusions may stabilize a hydrophilic pore (18), initiate a growth of tunnelling nanotubes (19–22), and affect endovesiculation (23,24) or membrane remodeling (25,26). It is hypothesized that incorporation of detergents and their association in the membrane will locally deform lipid bilayer structure by increasing positive local curvature of the binary mixture. More ordered membranes, such as those rich in long-saturated lipids and cholesterol, are less sensitive to solubilization (27).

In this work, we demonstrate a violent lipid vesicle dynamics and reshaping upon introduction of Triton X-100 (TR) detergent before giant 1,2-dioleoyl-*sn*-glycero-3-phosphocholine (DOPC) lipid vesicle solubilization. Shape changes were observed with confocal laser scanning fluorescence microscopy. The rates of flip-flop are known to be slow for artificial membranes, and thus, we assume that the induced spontaneous curvature is the prevailing mechanism driving shape change (28). Using Monte Carlo simulations, we show that vesicle reshaping can be reliably predicted by two parameters only: the concentration of the detergent incorporated into the lipid bilayer and the affinity between the curvophilic detergent molecules.

## MATERIALS AND METHODS

### Preparation of giant lipid vesicles

Giant DOPC lipid vesicles (GVs) were prepared by applying a rapid evaporation method as described by Moscho et al. (29). Briefly, DOPC was dissolved in chloroform to a concentration of 0.1 M. Then, 115  $\mu$ L of lipid solution was transferred into a 250 mL round-bottom flask containing 5.6 mL chloroform and 572  $\mu$ L methanol. Next, 40 mL buffer solution (10 mM HEPES buffer (pH 7.4)) with added fluorescein sodium salt (Thermo Fisher Scientific, Waltham, MA (0.3 mg/mL)) was carefully added along the flask walls to the lipid solution. Organic solvent was removed with a rotary evaporator (Büchi Rotavapor R-134, Büchi Waterbath B-480, Büchi Vacuum Controller V-850, Büchi Vacuum pump V-700; Büchi, Zagreb, Croatia) at 40 rotations per minute under reduced pressure (final pressure 55 mbar, volume flow rate 1.8 m<sup>3</sup>/h) in a water bath with temperature set at 40°C. Around the evaporation point of chloroform and methanol, we slowly reduced the pressure in 5 mbar increments to reach a gentle boiling point of solution. After reaching the final pressure of 55 mbar, the solution is left there for 2 min. In the next step, we separated vesicle fraction from the aqueous solution and excess fluorescein with centrifuging at 15,700  $\times g$  for 10 min. Lipid vesicles in the pellet were re-suspended in 40 mL 10 mM HEPES buffer. We repeated lipid vesicle washing three times, and after the third time, vesicles were concentrated into 5 mL HEPES buffer. For all experiments, the vesicles were freshly prepared. We used either fluorescein or rhodamine B as contrast agents packed in lipid vesicles. The final concentration of rhodamine B in 10 mM HEPES solution was 6 mg/mL. For vesicle membrane labeling, we used 3,3'-dioctadecyloxycarbocyanine perchlorate (DiO) lipophilic carbocyanine green fluorescent stain. Membrane-labeled vesicles were prepared as described above, with addition of 0.1 mol % DiO stain to DOPC mixture.

### Turbidity assay

A turbidity assay was performed as described by Ahyayauch et al. (30). Shortly, in a 96-well microtiter plate, 90  $\mu$ L of vesicle solution was mixed with 10  $\mu$ L of TR. The final detergent concentration gradient ranged from 0.03 to 1.7 mM. The mixtures were left to equilibrate for 10 min at room temperature, and solubilization was assessed from the changes in turbidity (Optical Density at 650 nm; OD650) and medium fluorescence intensity (excitation: 500 nm; emission: 530 nm). Measurements were made with a Biotek Cytation 3 microplate reader (BioTek, Winooski, VT).

### Microscopy

DOPC GVs were exposed to TR detergent under the microscope and monitored online to capture early lipid vesicle dynamics. In the experiments, the concentration of GV was between 10<sup>6</sup> and 10<sup>7</sup> vesicles/mL. All experiments were made under ambient conditions (room temperature, ambient air pressure). 9  $\mu$ L of vesicle solution was pipetted onto a #1.5 microscope coverglass to form a hemispheric drop after positioning and focusing the solution on the microscope, which was  $\sim$ 1  $\mu$ L of appropriate TR solution (final concentrations of TR were  $\sim$ 0.2 mM). Image acquisition started right after the addition of detergent.

Dynamics of lipid solubilization with TR was visualized with laser microscope fluorescence microscope Zeiss Axio Observer Z1 equipped with confocal unit LSM 800 (Carl Zeiss, Oberkochen, Germany). Fluorescein, rhodamine B, and DiO were excited with 488 nm laser wavelength. Image acquisition was under an immersion oil 100 $\times$  objective with additionally cropped view range. Because the vesicles were freely moving in a drop of solution and occasionally went out of focus, manual vesicle tracking was needed to acquire the full sequence of vesicle dynamics. For visualization of vesicle response to subsolubilization detergent concentration, critical micellar concentrations, and supercritical detergent concentrations, a 20 $\times$  objective was used.

## Theoretical model

When phospholipids can be idealized as a cylinder, as is the case for DOPC, the molecular volume is approximately equal to the product of the polar surface cross area and length of the hydrophobic chain. The packing parameter ( $p$ ) is then equal to 1 (9). Such amphiphiles are likely to form self-assembled flat bilayers because such packing entails a minimal exposure of hydrophobic chains to water. The molecular structure of TR, like most detergents, can be idealized as a cone. The volume of such a conical molecule is less than the product of the polar surface cross area and the length of the extended chain; therefore, its packing parameter is less than 1 (31). The exposure of hydrophobic chains is minimal when curved micelles are formed. A micelle has a spontaneous curvature that is by definition positive.

When phospholipid bilayers are mixed with a detergent, the two components are forced by entropy to reside in mixed aggregates. Before being solubilized, the bilayers retain their lamellar structure, but as the detergent/lipid ratio in the bilayers increases, detergent molecules agglomerate, leading to local membrane undulations.

In this model, the energy of a lipid vesicle is expressed as the sum of contributions of membrane bending and direct interactions between detergent inclusions (DI) embedded into the lipid membrane:

$$W = W_b + W_i, \quad (1)$$

where  $W_b$  is membrane bending energy and  $W_i$  is interaction between detergents. For the membrane bending energy, the standard Helfrich expression is used (32):

$$W_b = \frac{\kappa}{2} \int_A (C_1 + C_2 - C_0)^2 dA, \quad (2)$$

where the integral runs over the whole area of the membrane with bending stiffness  $\kappa$ ,  $C_1$  and  $C_2$  are the two principal curvatures, and  $C_0$  is the spontaneous curvature of the DI. On the patches occupied by the DIs, we therefore set  $C_0 = c_0$ , and elsewhere, we assume a symmetric membrane  $C_0 = 0$ . The DIs on the membrane are therefore modeled as isotropic patches of the membrane with given spontaneous curvature  $c_0$  (33–35). For patches occupied by the DIs, we set  $c_0 > 0$  because the positive sign of  $c_0$  means that the inclusions have a tendency to curve the membrane outwards. For direct interactions between neighboring DIs, we assume the step potential

$$W_i = -w \sum_{i < j} \mathcal{H}(r_0 - r_{ij}), \quad (3)$$

where  $w$  is a direct interaction constant, the sum runs over all DI pairs,  $r_{ij}$  are their mutual in-plane distances,  $\mathcal{H}(r)$  is the Heaviside step function, and  $r_0$  is the range of the direct interaction. We consider here attractive interactions  $w > 0$  that induce phase separation of the lipid bilayer (36).

## Monte Carlo simulations

The membrane is represented by a set of  $N$  vertices that are linked by tethers of variable length  $l$  to form a closed, dynamically triangulated, self-avoiding two-dimensional network of  $\sim 2N$  triangles and with the topology of a sphere (37,38). The lengths of the tethers can vary between a minimal and a maximal value,  $l_{min}$  and  $l_{max}$ , respectively. Self-avoidance of the network is ensured by choosing the appropriate values for  $l_{max}$  and the maximal displacement of the vertex  $s$  in a single updating step.

One Monte Carlo sweep (MCs) consists of individual attempts to displace each of the  $N$  vertices by a random increment in the sphere with radius  $s$ , centered at the vertex, followed by  $R_B N$  attempts to flip a randomly chosen bond. We denote  $R_B$  as the bond-flip ratio, which defines how many attempts to flip a bond are made per one attempt to

move a vertex in one MCs. Note that the bond-flip ratio is connected to the lateral diffusion coefficient within the membrane, i.e., to the membrane viscosity (39). In this work, we have chosen  $R_B = 3$ ,  $s/l_{min} = 0.15$ , and  $l_{max}/l_{min} = 1.7$ . The dynamically triangulated network acquires its lateral fluidity from a bond-flip mechanism. A single bond flip involves the four vertices of two neighboring triangles. The tether connecting the two vertices in diagonal direction is cut and reestablished between the other two previously unconnected vertices. The self-avoidance of the network is implemented by ensuring that no vertex can penetrate through the triangular network and that no bond can cut through another bond.

The microstates of the membrane are sampled according to the Metropolis algorithm. The probability of accepting the change of the microstate due to vertex move or bond flip is  $\min[1, \exp(-\Delta E/kT)]$ , where  $\Delta E$  is the energy change,  $k$  is the Boltzmann constant, and  $T$  is absolute temperature. The energy for a given microstate is specified by Eq. 1. The bending energy is discretized as described by Gompper and Kroll (37,38). For each set of parameters, the system is initially thermalized. Ensemble averaging is done over 200 statistically independent microstates.

In this work, we set  $N_d$  of the total  $N = 1447$  vertices to represent DIs, which have spontaneous curvature  $c_0$  in the range between  $c_0 = 0$  (for flat proteins) and  $c_0 = 1/l_{min}$  for the most highly curved proteins that can be described well by the discrete mesh. For clarity, the explicit dimension of curvature is omitted throughout the text. All other vertices represent symmetric membrane and have zero spontaneous curvature. The fraction of curved inclusions on the membrane is given by

$$\rho = \frac{N_d}{N} \quad (4)$$

It should be noted that  $\rho$  does not represent a molar fraction of detergent added to the solution of GVs directly, albeit being proportional to it. Rather,  $\rho$  serves as a qualitative measure of TR molecules found in the membrane and serves as the main parameter characterizing simulated vesicle morphologies.

We assume that the detergent binds to the membrane in a gradual process, which is accounted for in the simulations by an addition of a fraction of  $N_d$  DIs into the mesh every iteration at random positions on the mesh. The rate of inclusion addition is the same for all inclusion densities but varies from three to six to ensure the same simulation times. After each iteration, 2000 MCs are performed before new DIs are added again and the process is repeated. This gradual addition is crucial to account for the metastability of the process, as detergent-phospholipid mixtures may be stable for long periods of time without being at equilibrium (17). After the total number of DI  $N_d$  is reached, an additional 50 iterations with no new added DIs are performed with the aim of relaxing the energy of the final state even further. A typical simulation includes around 350 iterations and takes around 10 min to execute on a laptop with eight IntelCore i7-8550U cores.

It should be noted that the length of the simulation is determined experimentally; seeing that stable equilibrium shapes after adding all the inclusions at once are attained after around 300 iterations, this sets a benchmark for the cases of gradual adding of inclusions.

If the two vertices representing the DI are nearest neighbors, there is an additional energy term  $w$  assigned to their bond. The direct interaction constant  $w$  is assumed to be of the order of the thermal energy  $kT$ , where  $T_0 = 300$  K is room temperature, and the membrane bending stiffness  $\kappa$  is of the order of  $20 kT_0$ .

After a constant number of vertices in the discrete mesh is set ( $N = 1447$ ), the phase space of the Monte Carlo simulations consists of three independent parameters: proportion of curved inclusions ( $\rho$ ), spontaneous curvature of the curved inclusions ( $c_0$ ), and the nearest neighbor interaction constant ( $w$ ). To reflect the physical phenomena of the studied system of vesicles, these parameters have to be considered within approximate bounds. The proportion of curved inclusions ( $\rho$ ) varies from 0.28 to 0.8.

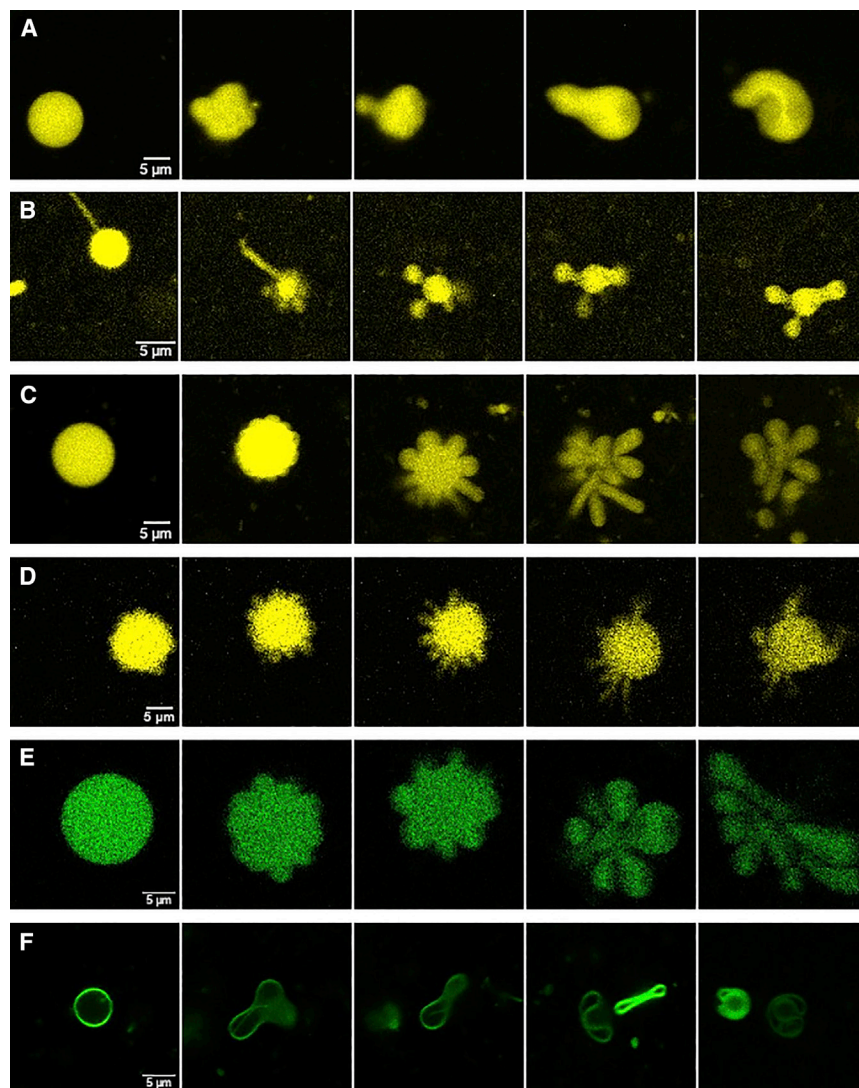


FIGURE 1 Microscopic image sequence of DOPC vesicle upon addition of TR under confocal fluorescence microscope. (A–D) represent different sequences of vesicle shape change in the experiments. Vesicles were packed with fluorescein (yellow pseudocolor). (E) is an image sequences of a vesicle packed with rhodamine B (green pseudocolor), which showed similar vesicle dynamics as fluorescein-packed vesicles. (F) shows a sequence of vesicle shape dynamics after addition of TR to a DiO membrane-labeled vesicle. To see these figures in color, go online.

## RESULTS

### DOPC and Triton X-100 experiments

The reshaping of DOPC lipid vesicles after the addition of TR is shown in Fig. 1. The initial shape of the vesicles before TR addition was spherical, as is apparent in the first column of Fig. 1. The vesicle lumen was contrasted with either fluorescein or rhodamine B and observed in confocal mode to enhance the resolution. After addition of the detergent, the spherical vesicle shape begins to deform. The dynamics of individual lipid vesicles is shown in time-lapse videos (Videos S1, S2, S3, S4, S5, and S6). Different patterns (shape families) were observed upon introduction of the detergent. A minority of lipid vesicles had a moderate shape change (Fig. 1 A). The lipid vesicles changed from spherical to cylindrical or became toroidal. A different sequence of shape changes was observed in Fig. 1 B, in which vesicles changed from spherical to pear-like struc-

tures with two unequal lobes, with one of the lobes—usually the smallest—potentially infolding. A large proportion of vesicles showed nanotube-like protrusions upon detergent addition, which could be classified into three patterns: 1) vesicles with a single very long nanotube extending several micrometers from the surface of the lipid vesicle (Fig. 1 C), 2) vesicles with several large protrusions (Fig. 1 D), and 3) lipid vesicles with many small nanotube protrusions of different length (Fig. 1 E). The fluorescence-labeled lipid vesicles were also subject to detergent solubilization, as were lipid vesicles labeled with fluorescein. There was a moderate shape change after detergent injection, with many similar morphological features as observed in fluorescein-labeled vesicles (Fig. 1 F).

The response of DOPC vesicles to different concentrations of added TR detergent is shown in Fig. S1. From the turbidity assay (Ahyayauch et al. (30)), it can be seen that at low detergent concentrations, OD650 values did not

change significantly, then increased at around the detergent critical micelle concentration, and thereafter decreased as a result of vesicle solubilization. With increasing detergent concentrations, there was a steady increase of fluorescence intensity, which suggests vesicle leakage. When all vesicles were solubilized, the fluorescence intensity reached a steady-state value. The red vertical band in Fig. S1 represents the detergent concentrations at which our experiments with vesicle dynamical shape changes were performed.

Additionally, we observed vesicle dynamics at different detergent concentrations (Videos S7, S8, and S9). In Video S7, there is a time-lapse sequence of vesicles immediately after the addition of the detergent at a subsolubilizing concentration of 0.03 mM. After the initial disturbance due to the detergent injection, no significant difference in vesicle shape could be observed in a given time frame (20 min). Vesicles did not solubilize during this time period. When a critical micellar concentration of 0.22 mM was added (Video S8), we observed a gradual change of vesicle shapes until the majority of vesicles solubilized. When we added a supercritical detergent concentration of 1.7 mM (Video S9), a rapid vesicle solubilization was observed in the direction of detergent front progression. Although vesicle shape dynamics could be observed, the dynamics was so rapid that it was visible only on a couple of frames. From these experiments, the outline of the dynamic phase diagram can be glimpsed. Obviously, the detergent concentration gradient has a significant impact on vesicle dynamic shape morphology and solubilization rate. With gradual DI inserted into the lipid bilayer, different vesicle shapes can be observed, whereas a large number of DI in a short time interval result in fast vesicle solubilization. To be able to see the observed vesicle shape dynamic, the detergent concentration is absolutely critical. Adding too little or too much detergent will either abolish morphological changes or speed up morphological changes and cause vesicle solubilization before recognizing shape dynamics. This is likely the reason why other researchers fail to notice the rapid vesicle shape dynamics upon detergent addition.

Although crossover between different shapes was observed, the vesicles mostly stayed within a given shape family. The vesicles of a given shape family, in particular those with small and large nanotube protrusions, were oscillating violently between different subshapes, making asymmetric stretches, twists, kick steps, jumps, throws, and flips. In general, the motion of the lipid vesicle surface could be described as the “rocking and rolling” of a ship on the rough lipid ocean.

The observed morphological dynamics is very likely the result of the local detergent concentration. When the injected detergent concentration was high, the dynamics in the whole experimental system was so fast that we were not able to resolve the violent morphological fluctuations before the vesicle solubilization. On the other hand,

if the injected detergent concentration was low, the morphology did not change sufficiently during the experiment. The injected TR concentration in our experiments was  $\sim 0.2$  mM, which is just below its critical micelle concentration (CMC). Only when the ratio of lipid/injected detergent was around 50:1 could we observe the morphological fluctuation dynamics. Because detergent was added locally and not mixed, the system did not reach equilibrium before the onset of morphological fluctuations. Most notably, the time of violent morphological changes varied between different vesicles (from 30 s up to 5 min). Once initiated, the morphological fluctuations in different vesicles followed similar paths. Because lipid vesicles were distributed at different distances from the detergent injection site, they could accumulate different concentrations of detergents and therefore follow different morphological sequences.

### Monte Carlo simulation results

The results of Monte Carlo simulations are given in Fig. 2. Overall, the results of simulations reproduce very well the main patterns of vesicle behavior observed upon detergent addition (i.e., formation of spheroids, irregular structures, pear-like shapes, lobed structures, and nanotube-like protrusions). The final simulated microstates obtained after the gradual addition of detergent were dependent on the density of DIs ( $\rho$ ), the association between the detergent molecules ( $w$ ), and the curvature of the DI ( $c_0$ ). As given in Fig. 2, both the detergent density and the interaction between detergents have a major effect on the lipid vesicle shape. At low interactions between detergent molecules (i.e.,  $w = 0.5$ ), the increasing detergent concentration decreased the flat membrane patches and the vesicle shapes become irregular, sometimes with necklace-like protrusions that are commonly observed in vesicle systems (40). The vertices of the irregular vesicle shape were composed mainly of the detergent molecules. At detergent concentrations  $\rho > 0.6$ , the percolation threshold has been reached and the majority of the detergent molecules were interconnected. When the association between the detergent molecules was high (i.e.,  $w = 2$ ), the shape of the lipid vesicle became distorted already at much lower detergent concentrations. The vesicle structure evolved quickly into a lobed structure with increasing detergent concentration, and vesicles had a significantly increased surface/volume ratio. The detergent density was simulated from 0.28 to 0.8. Below  $\rho = 0.28$ , there were not enough curved DIs to have a significant effect on morphology, and vesicles generally retain their quasi-spherical shape. On the other hand, we found that at  $\rho > 0.8$ , vesicle shapes become pronouncedly spiculated and branched, with high local curvature. This should, in principle, initiate the pinching of detergent-loaded lipid micelles and start the solubilization of the lipid vesicle. Because the simulations did not include tearing of the membrane,

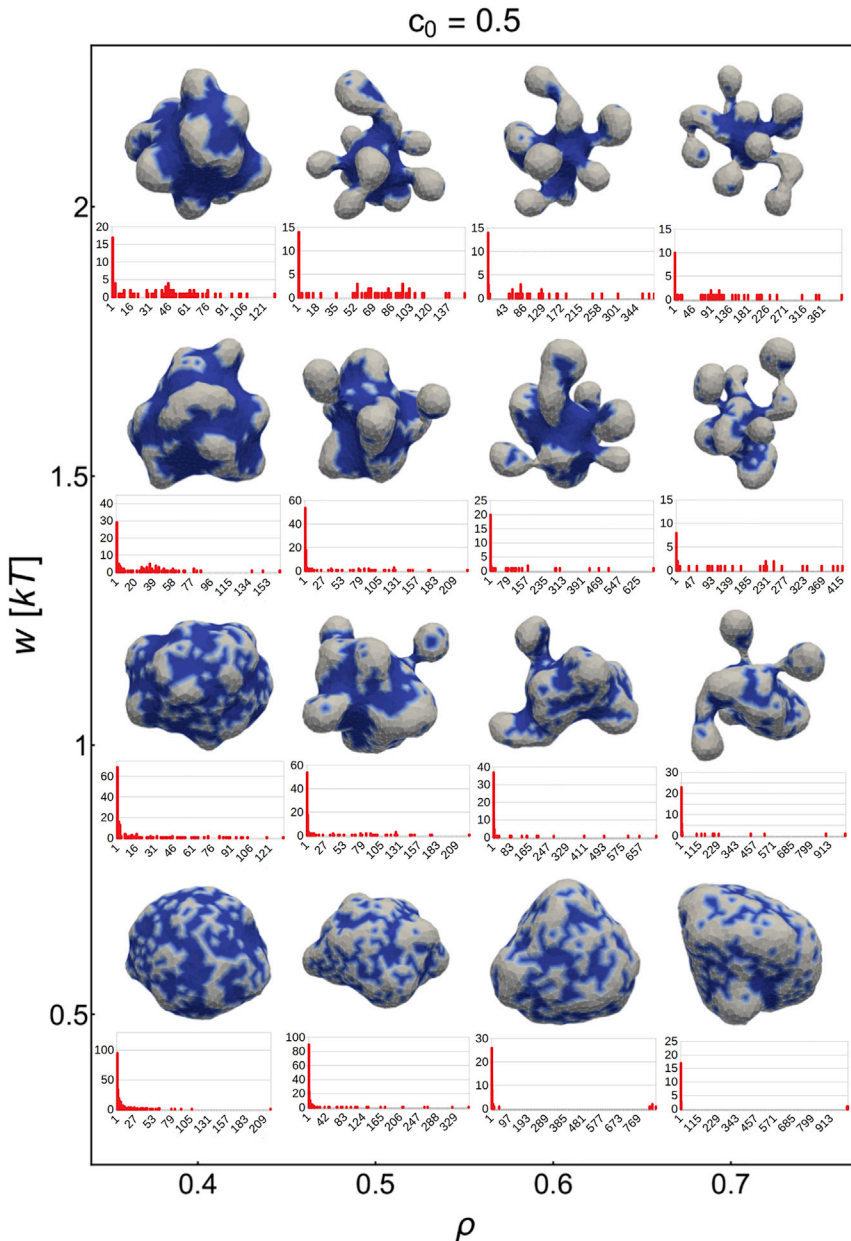


FIGURE 2 Final microstates of vesicles for gradual adding of curved inclusions ( $N_d$ ) every five iterations for  $c_0 = 0.5$ . The patches of flat membrane with no spontaneous curvature are shown in dark blue, and the gray areas correspond to positive spontaneous curvature  $c_0$  at which curved inclusions are present. In the corresponding cluster-size distributions, the y axis is the number of curved inclusions of each size, and the x axis is the curved inclusion cluster size as a sum of five simulations at given parameters. There were 300 iteration steps for each snapshot. To see these figures in color, go online.

we have limited the simulation up to and including a detergent density of  $\rho = 0.8$ .

To test the sensitivity of the simulation parameters, we have made several phase portraits for different model conditions. Fig. 3 shows a phase portrait of simulated vesicles at a constant curvature and association between the detergent molecules (i.e.,  $c_0 = 0.5$ ,  $w = 2$ ) at different detergent densities with increasing number of iteration steps. At low detergent concentration (i.e.,  $\rho = 0.4$ ), the increased number of iteration steps did not change the morphology of the lipid vesicle, although detergent molecules aggregated with increasing number of iteration steps and formed patches. The concave vesicles start to appear when detergent concen-

tration gradually increased. The effect of increasing  $w$  correlates with the homogeneity of inclusion distribution, whereas increasing densities  $\rho$  result in more highly curved parts of the vesicle that bend outwards to accommodate for the spontaneous curvature of the inclusions. Protrusion growth was pronounced only at  $\rho > 0.5$  and  $w > 0.5$ , at which these two effects amplify budding of the membrane in a process that resembles vesiculation. Because the simulations did not account for membrane fission, the limit of such a vesiculation process result in highly tubular, branched morphologies at higher number of iteration steps. The vesiculation process can be followed with vesicle volume decrease (Fig. 3 D) and a concomitant increase of the

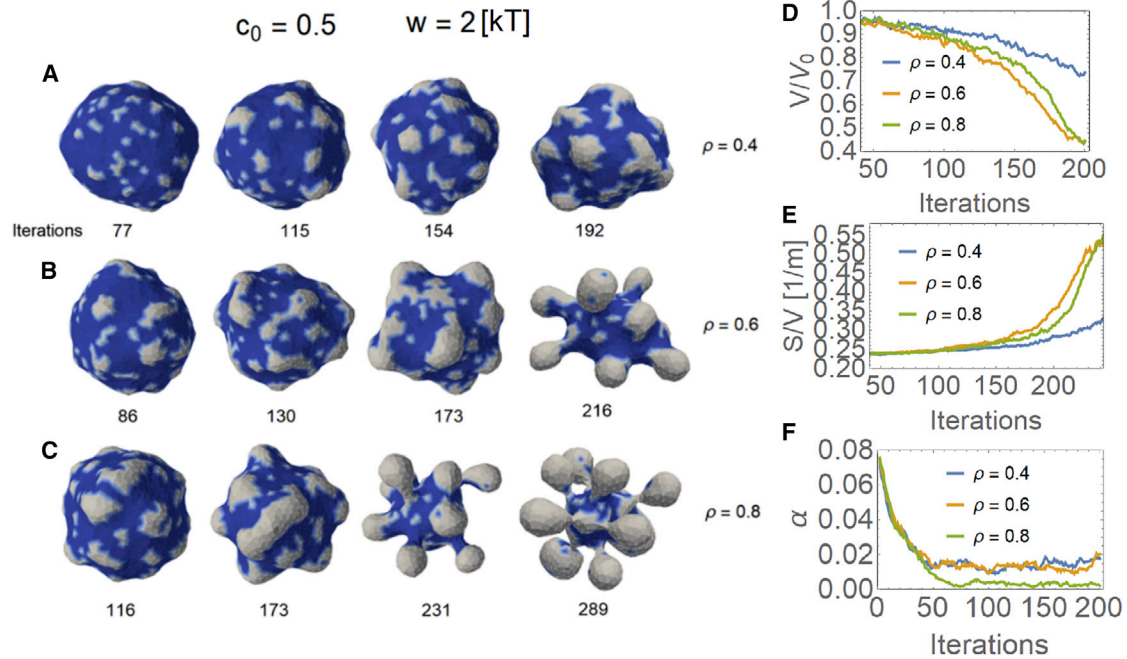


FIGURE 3 Sequential microstates of vesicles with an increasing number of curved inclusions ( $c_0 = 0.5$ ) on the membrane (marked as *gray areas* of the surface) for different end concentrations of inclusions  $\rho = 0.4$ ,  $\rho = 0.6$ , and  $\rho = 0.8$  for (A), (B), and (C), respectively. With increasing number of iteration steps, the reduced volume decreases (D), whereas the surface/volume ratio increases (E). (F) The asphericity  $\alpha$  as defined by Eq. 4. In all cases,  $w = 2$ . To see these figures in color, go online.

surface/volume ratio (Fig. 3 E). At low detergent concentrations, the vesiculation was indicated only at a very high number of iteration steps. Conversely, at high detergent concentrations ( $\rho > 0.5$ ), the surface/volume ratio increased at significantly lower number of iteration steps.

In general, with passing iteration steps, curved inclusions start to aggregate and form patches of the membrane with a preferred spontaneous curvature, leading to a formation of undulations and buds. Any deviation from quasispherical shapes leads to a decrease in volume and an increase of the surface/volume ratio. The change of vesicle shape could be assessed by calculating the asphericity parameter  $\alpha$ . Asphericity is the degree of deviation from a spherical shape, calculated as (41)

$$\alpha = \frac{(\lambda_1 - \lambda_2)^2 + (\lambda_2 - \lambda_3)^2 + (\lambda_3 - \lambda_1)^2}{2(\lambda_1 + \lambda_2 + \lambda_3)^2}, \quad (5)$$

where  $\lambda_i$  are the eigenvalues of the gyration tensor of the vesicle. For the thin rod limit,  $\alpha = 1$  ( $\lambda_1 = 1$ ,  $\lambda_2 = \lambda_3 = 0$ ), whereas  $\alpha = 0.25$  for disks. When the vesicle forms three or four spindles,  $\alpha$  starts to decrease (Fig. 3 F).

In the experiments, the concentration of detergent molecules in the membrane increased with time. In simulations, we have accounted for this by gradual addition of curved DI after every iteration. This was done to mimic the highly metastable and dynamic nature of the solubilization process and to allow shapes to attain the energy minima. To check

whether gradual incorporation of detergents is important for the outcome of the simulation, we have simulated the situation in which all curved DI were added at once to the lipid bilayer before the first iteration step. The phase portrait is given in Fig. 4. It is instructive to compare the gradual addition of detergent (Fig. 2) to the complete addition (Fig. 4). At low detergent interaction energy (i.e.,  $w = 0.5$ ), vesicle shapes stayed quasispherical for the gradual case but were highly branched and tubular for the complete detergent addition after the same number of iteration steps.

The shapes in gradual detergent additions start minimizing their bending energy when there are few curved inclusions present in the membrane, retaining their spherical morphology even after new inclusions were added to the surface. In complete detergent addition before the simulations (Fig. 4), curved inclusions start grouping together from the start of the simulation and formed patches of curved membrane that accumulated, resulting in highly curved morphologies that form spindles. In terms of cluster distributions of DIs, we see that gradual addition resulted in a diverged grouping: either most DIs were present in small patches, or they were a part of a superpatch containing almost all DIs on the membrane. In comparison, in the case of complete detergent addition, more medium-sized patches formed that evolved to membrane buds. These differences persisted even at larger  $w$  and  $\rho$ . Shapes obtained by gradual addition generally had thicker buds and protrusions, with a more pronounced central region of the membrane devoid of curved inclusions (Fig. 2), as opposed to

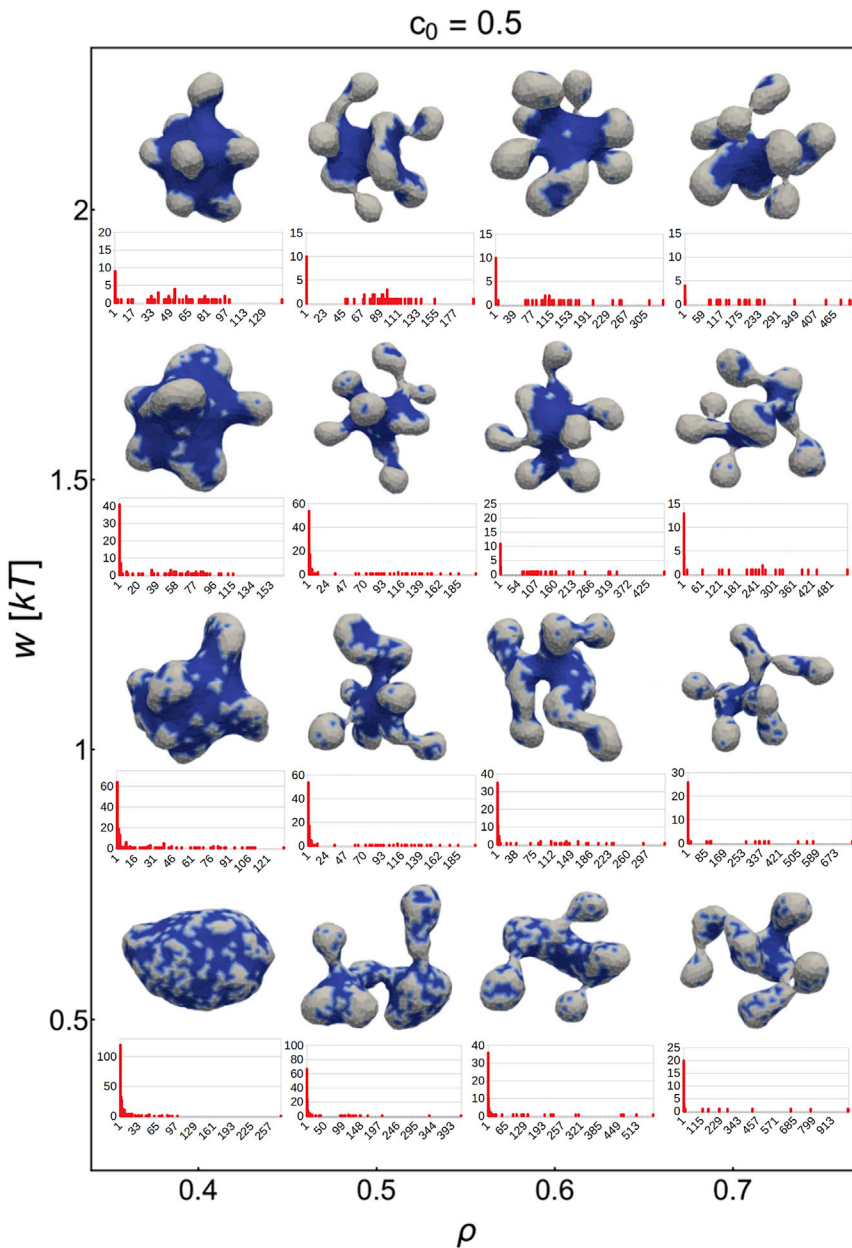


FIGURE 4 Final microstates of vesicles for which all curved inclusions ( $N_d$ ) were added before the first iteration for  $c_0 = 0.5$ . The patches of flat membrane with no spontaneous curvature are shown in dark blue, and the gray areas correspond to positive spontaneous curvature  $c_0$  at which curved inclusions are present. In the corresponding cluster-size distributions, the y axis is the number of curved inclusions of each size, and the x axis is the curved inclusion cluster size as a sum of five simulations at given parameters. Note the tubular worm-like structures lacking a centralized bulk vesicle usually present in gradual addition snapshots (Fig. 2). There were 300 iteration steps for each snapshot. To see these figures in color, go online.

shapes obtained by adding all detergent at once (Fig. 4). The latter were also more prone to resembling tubular structures with no apparent central part from which undulations emanated, a trait that was observed in nearly all shapes upon gradual detergent addition. This is due to the fact that curved inclusions are always added to the vacant positions on the surface and are therefore more likely to be locally flat. However, the complete addition of the detergent before the simulation can fall quickly into a kinetic trap, a relatively stable but not true equilibrium state, resulting in shapes that only elongate with more iterations, with much thinner necks connecting buds to the central shape (Fig. 4).

In conclusion, comparing the results of the simulation (Figs. 2 and 4) with the experimental results of detergent addition (Fig. 1), it is clear that the simulation with a gradual addition of detergents much better describes the dynamic evolution of lipid shapes than the simulation with complete detergent addition before the simulation.

The spontaneous curvature of DIs in the lipid bilayer is not known exactly. The results of simulating an increasing detergent spontaneous curvature are given in Fig. 5. It is important to note that spontaneous curvature  $c_0$  equal to zero leads to a trivial result yielding perfectly spherical vesicles. The increased detergent-inclusion curvature can have a pronounced effect on lipid vesicle shape already at low

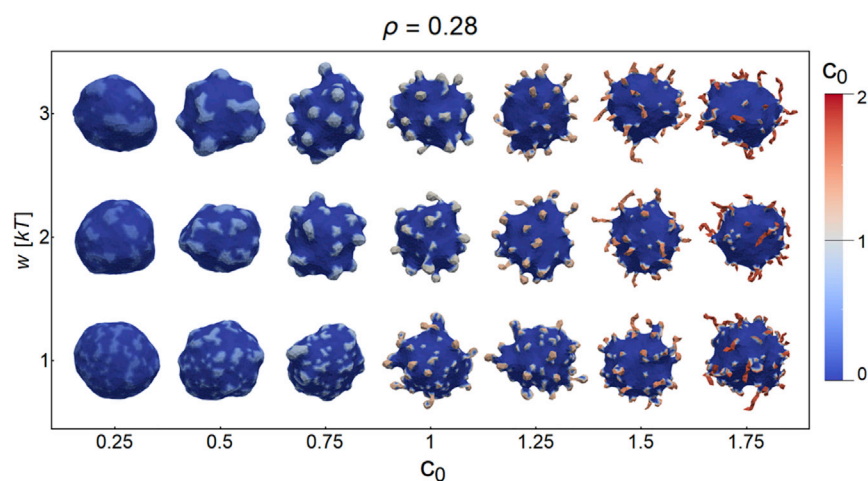


FIGURE 5 Snapshots of vesicle microstates for  $\rho = 0.28$ . The patches of flat membrane with no spontaneous curvature are shown in dark blue, and the heatmap colors correspond to areas of positive curvature where curved inclusions are present. The interaction parameter  $w$  regulates the homogeneity of the curved inclusion domains; at values  $w = 1$ , the interaction is relatively weak, resulting in a homogeneous distribution of inclusions across the vesicle, whereas increasing  $w$  results in more localized patches of curved membrane. Coupling this effect with high spontaneous curvature of inclusions results in the formation of protrusions shown in red. There were 300 iteration steps for each snapshot. To see these figures in color, go online.

detergent concentrations (i.e.,  $\rho = 0.28$ ). With increasing curvature, the number of protrusions increases. We have limited the simulations to values of  $c_0 < 1$  to avert from discontinuities. Theoretically, the highest possible  $c_0 = 1/l_{min}$ . The detergent neighbor interaction  $w$  was hardest to approximate because mechanisms of curved inclusion attraction are not well known. We found that an increasing  $w$  facilitates protrusion growth because it minimizes total energy but also regulates the homogeneity of the curved protrusion domains across the membrane.

## DISCUSSION

The structural changes of liposome-induced solubilization by detergents have been known experimentally for some time and take various solubilization pathways depending on the types of lipids and detergents. The morphology changes include shrinkage, bursting, budding, fission, peeling, and inside-out inversion. The equilibrium interactions between detergents and phospholipid bilayers (i.e., phase diagrams) have also been described (2,42). In the mixed system composed of lipids and detergents in aqueous solutions, the phase boundaries describe the range of partial lipid solubilization structures. A general consensus is that lipid bilayer solubilization proceeds in three stages (43). In stage 1, detergent partition between lipid bilayers and the aqueous media occurs, and in stage 2, a composition-induced disintegration of the bilayers forms long thread-like mixed micelles. In stage 3, at higher detergent concentrations, solubilization is followed by an entropy-derived rapid series of mixing large detergent-phospholipid mixed micelles with pure detergent micelles, yielding smaller mixed micelles with a higher detergent/phospholipid ratio. Theoretical approaches to the self-assembly of binary surfactant mixtures were mostly studied in stage 3 (43) with the onset of micellization and pore formation, but little is known about the mechanisms of membrane structural

changes in the intermediate stage, at which the binary mixtures coexist and the topology of the vesicles is not yet compromised. In particular, very little is known about structural behavior under nonequilibrium conditions, in which constant influx of detergent molecules introduces nonlinear dynamics in the lipid bilayer.

In this work, a possible mechanism of membrane structural changes seen in experiments with DOPC liposomes and TR mixtures before solubilization is presented within a simple Monte Carlo model. In the model, curved DI move laterally in the membrane and induce local curvature changes because of their molecular shape. This leads to a “rock-and-roll” dynamics of lipid vesicles seen in the experiments before micellization and solubilization of liposomes. Morphology changes observed in the experiments and simulations alike encompass symmetry breaking, resulting in protrusion growth and undulating geometries. The simulation qualitatively predicts the observed dynamic morphology changes up to a point of pore formation and micellization of the vesicles. It is found that the metastability of the process in the simulation is of crucial importance in predicting the three-dimensional shapes of lipid vesicles.

To our knowledge, such simulations are novel and predict morphology changes before pore formation and the total solubilization of liposomes. In future work, it would be interesting to couple the simulation parameters with differential scanning calorimetry (DSC), isothermal titration calorimetry, or infrared or NMR spectrometry results to study the effect of phase transitions of lipids in the membrane. To our knowledge, past studies tended to focus on the phase diagrams of late stages of solubilization with steady-state fluorescence spectroscopy (44) or isothermal titration calorimetry (45). Our findings are in line with recent molecular dynamics simulations of liposomes and detergents, which confirmed that the detergent adsorption induces spontaneous curvature of the vesicle bilayer, resulting in thin

neck formations connecting smaller spherical vesicles (46,47).

Lipid vesicles have been used extensively to understand the equilibrium and nonequilibrium dynamics of simplified biological cells that do not contain a cytoskeleton or have protein-loaded membrane. The results obtained in this study are therefore of interest for cell biology. The cells are regularly challenged by amphiphiles, which may induce lipid phase transition, cell shape alteration, and ultimately cell death (48,49). On the other hand, cells may autonomously control amphiphile concentration in the lipid bilayer (i.e., lysolipids) and thereby induce local or global shape change (14). Another venue in which one could benefit from the knowledge of nonequilibrium dynamics before solubilization is triggered liposome release of cargo in biomedical applications such as drug delivery and micro- or nanoscale reactors (50).

## CONCLUSION

In this work, the interaction between DOPC giant vesicles and nonionic detergent Triton X-100 was studied, with an emphasis on the processes before the solubilization. Intensive and dynamic changes of DOPC liposome morphology were observed. A possible mechanism for such a dynamic process is proposed that is based on the geometrical and associative properties of the detergent molecules that are adsorbed and laterally diffuse across the lipid vesicle. Three-dimensional Monte Carlo numerical simulations were used to study the phase space of metastable shapes, their dependence on detergent-inclusion spontaneous curvature, and the attraction between detergent molecules under nonequilibrium detergent concentrations. It is found that the gradual addition of curved detergent inclusions predicts very well the morphological shapes observed in experiment (spheroids, pears, undulations, lobes, spicules, and budding vesicles with thin necks connecting regions of quasispherical vesicles). The results are in line with the existing literature and shed a new, to our knowledge, light on the mechanical and dynamical aspects of the early stages of the solubilization process.

## SUPPORTING MATERIAL

Supporting material can be found online at <https://doi.org/10.1016/j.bpj.2021.09.005>.

## AUTHOR CONTRIBUTIONS

M.D.: investigation, methodology, visualization, writing—original draft, and writing—review and editing. Z.P.: investigation, methodology, and writing—review and editing. S.P.: methodology and visualization. A.I.: conceptualization, supervision, and writing—review and editing. V.K.-I.: conceptualization, supervision, and writing—review and editing. D.S.: supervision, conceptualization, methodology, and writing—review and editing.

## ACKNOWLEDGMENTS

The authors are thankful to Professor Nir Gov for ideas that improved the manuscript.

We acknowledge the financial support from the research programs nos. P2-0232 and P3-0388 and research projects nos. J3-9262, J3-2533, L3-2621, and J1-9162, all from the Slovenian Research Agency. We also acknowledge the funding from the European Union's Horizon 2020 research and innovation programme VES4US No. 801338.

## REFERENCES

1. Kumar, D., C. M. Richter, and C. M. Schroeder. 2020. Conformational dynamics and phase behavior of lipid vesicles in a precisely controlled extensional flow. *Soft Matter*. 16:337–347.
2. Tomita, T., T. Sugawara, and Y. Wakamoto. 2011. Multitude of morphological dynamics of giant multilamellar vesicles in regulated nonequilibrium environments. *Langmuir*. 27:10106–10112.
3. Babnik, B., D. Miklavčič, ..., A. Iglič. 2003. Shape transformation and burst of giant POPC unilamellar liposomes modulated by non-ionic detergent C12E8. *Chem. Phys. Lipids*. 125:123–138.
4. Mavčič, B., B. Babnik, ..., V. Kralj-Iglič. 2004. Shape transformation of giant phospholipid vesicles at high concentrations of C12E8. *Bioelectrochemistry*. 63:183–187.
5. Peterlin, P., V. Arrigler, ..., P. Walde. 2009. Growth and shape transformations of giant phospholipid vesicles upon interaction with an aqueous oleic acid suspension. *Chem. Phys. Lipids*. 159:67–76.
6. Dervaux, J., V. Noireaux, and A. Libchaber. 2017. Growth and instability of a phospholipid vesicle in a bath of fatty acids. *Eur. Phys. J. Plus*. 132:1–10.
7. Tanford, C. 1980. *The Hydrophobic Effect: Formation of Micelles and Biological Membranes*, Second Edition. J. Wiley, New York.
8. Heerklotz, H., and R. M. Epand. 2001. The enthalpy of acyl chain packing and the apparent water-accessible apolar surface area of phospholipids. *Biophys. J.* 80:271–279.
9. Israelachvili, J. N. 2015. *Intermolecular and Surface Forces*. Academic Press, London.
10. Lombardo, D., M. A. Kiselev, ..., P. Calandra. 2015. Amphiphiles self-assembly: basic concepts and future perspectives of supramolecular approaches. *Adv. Condens. Matter Phys.* 2015:151683.
11. Andersen, O. S., and R. E. Koeppe, II. 2007. Bilayer thickness and membrane protein function: an energetic perspective. *Annu. Rev. Biophys. Biomol. Struct.* 36:107–130.
12. McIntosh, T. J., and S. A. Simon. 2006. Roles of bilayer material properties in function and distribution of membrane proteins. *Annu. Rev. Biophys. Biomol. Struct.* 35:177–198.
13. Iglič, A., D. Drobne, and V. Kralj-Iglič. 2015. *Nanostructures in Biological Systems: Theory and Applications*. CRC Press, Boca Raton, FL.
14. Fuller, N., and R. P. Rand. 2001. The influence of lysolipids on the spontaneous curvature and bending elasticity of phospholipid membranes. *Biophys. J.* 81:243–254.
15. Mesarec, L., M. Drab, ..., A. Iglič. 2021. On the role of curved membrane nanodomains, and passive and active skeleton forces in the determination of cell shape and membrane budding. *Int. J. Mol. Sci.* 22:2348.
16. Kralj-Iglič, V., B. Babnik, ..., A. Iglič. 2006. Quadrupolar ordering of phospholipid molecules in narrow necks of phospholipid vesicles. *J. Stat. Phys.* 125:727–752.
17. Lichtenberg, D., H. Ahyayauch, and F. M. Goñi. 2013. The mechanism of detergent solubilization of lipid bilayers. *Biophys. J.* 105:289–299.
18. Fošnarič, M., V. Kralj-Iglič, ..., S. May. 2003. Stabilization of pores in lipid bilayers by anisotropic inclusions. *J. Phys. Chem. B.* 107:12519–12526.

19. Kralj-Iglič, V., A. Iglič, ..., P. Peterlin. 2000. Stable tubular microexovesicles of the erythrocyte membrane induced by dimeric amphiphiles. *Phys. Rev. E Stat. Phys. Plasmas Fluids Relat. Interdiscip. Topics.* 61:4230–4234.
20. Kralj-Iglič, V., H. Hägerstrand, ..., A. Iglič. 2005. Amphiphile-induced tubular budding of the bilayer membrane. *Eur. Biophys. J.* 34:1066–1070.
21. Drab, M., D. Stopar, ..., A. Iglič. 2019. Inception mechanisms of tunneling nanotubes. *Cells.* 8:626.
22. Mahapatra, A., C. Uysalel, and P. Rangamani. 2021. The mechanics and thermodynamics of tubule formation in biological membranes. *J. Membr. Biol.* 254:273–291.
23. Bobrowska-Hägerstrand, M., V. Kralj-Iglič, ..., H. Hägerstrand. 1999. Torocyte membrane endovesicles induced by octaethyleneglycol dodecylether in human erythrocytes. *Biophys. J.* 77:3356–3362.
24. Auth, T., and G. Gompper. 2009. Budding and vesiculation induced by conical membrane inclusions. *Phys. Rev. E Stat. Nonlin. Soft Matter Phys.* 80:031901.
25. Atilgan, E., and S. X. Sun. 2007. Shape transitions in lipid membranes and protein mediated vesicle fusion and fission. *J. Chem. Phys.* 126:03B604.
26. Reynwar, B. J., G. Illya, ..., M. Deserno. 2007. Aggregation and vesiculation of membrane proteins by curvature-mediated interactions. *Nature.* 447:461–464.
27. Sot, J., L. A. Bagatolli, ..., A. Alonso. 2006. Detergent-resistant, ceramide-enriched domains in sphingomyelin/ceramide bilayers. *Biophys. J.* 90:903–914.
28. Sudbrack, T. P., N. L. Archilha, ..., K. A. Riske. 2011. Observing the solubilization of lipid bilayers by detergents with optical microscopy of GUVs. *J. Phys. Chem. B.* 115:269–277.
29. Moscho, A., O. Orwar, ..., R. N. Zare. 1996. Rapid preparation of giant unilamellar vesicles. *Proc. Natl. Acad. Sci. USA.* 93:11443–11447.
30. Ahyauch, H., M. I. Collado, ..., F. M. Goñi. 2012. Lipid bilayers in the gel phase become saturated by triton X-100 at lower surfactant concentrations than those in the fluid phase. *Biophys. J.* 102:2510–2516.
31. Israelachvili, J. N., S. Marčelja, and R. G. Horn. 1980. Physical principles of membrane organization. *Q. Rev. Biophys.* 13:121–200.
32. Helfrich, W. 1973. Elastic properties of lipid bilayers: theory and possible experiments. *Z. Naturforsch. C.* 28:693–703.
33. Iglič, A., T. Slivnik, and V. Kralj-Iglič. 2007. Elastic properties of biological membranes influenced by attached proteins. *J. Biomech.* 40:2492–2500.
34. Iglič, A., M. Lokar, ..., V. Kralj-Iglič. 2007. Possible role of flexible red blood cell membrane nanodomains in the growth and stability of membrane nanotubes. *Blood Cells Mol. Dis.* 39:14–23.
35. Fošnarič, M., S. Penič, ..., N. S. Gov. 2019. Theoretical study of vesicle shapes driven by coupling curved proteins and active cytoskeletal forces. *Soft Matter.* 15:5319–5330.
36. Veksler, A., and N. S. Gov. 2007. Phase transitions of the coupled membrane-cytoskeleton modify cellular shape. *Biophys. J.* 93:3798–3810.
37. Gompper, G., and D. Kroll. 1996. Random surface discretizations and the renormalization of the bending rigidity. *J. Phys. I.* 6:1305–1320.
38. Gompper, G., and D. Kroll. 2004. Triangulated-surface models of fluctuating membranes. In *Statistical Mechanics of Membranes and Surfaces.* D. Nelson, T. Piran, and S. Weinberg, eds. World Scientific, pp. 359–426.
39. Bivas, I., P. Hanusse, ..., O. Aguerre-Chariol. 1987. An application of the optical microscopy to the determination of the curvature elastic modulus of biological and model membranes. *J. Phys. (Paris).* 48:855–867.
40. Bhatia, T., S. Christ, ..., R. Lipowsky. 2020. Simple sugars shape giant vesicles into multispheres with many membrane necks. *Soft Matter.* 16:1246–1258.
41. Rudnick, J., and G. Gaspari. 1987. The shapes of random walks. *Science.* 237:384–389.
42. Arnulphi, C., J. Sot, ..., F. M. Goñi. 2007. Triton X-100 partitioning into sphingomyelin bilayers at subsolubilizing detergent concentrations: effect of lipid phase and a comparison with dipalmitoylphosphatidylcholine. *Biophys. J.* 93:3504–3514.
43. Helenius, A., and K. Simons. 1975. Solubilization of membranes by detergents. *Biochim. Biophys. Acta.* 415:29–79.
44. Juan-Colás, J., L. Dresser, ..., S. D. Quinn. 2020. The mechanism of vesicle solubilization by the detergent sodium dodecyl sulfate. *Langmuir.* 36:11499–11507.
45. Heerklotz, H., A. D. Tsamaloukas, and S. Keller. 2009. Monitoring detergent-mediated solubilization and reconstitution of lipid membranes by isothermal titration calorimetry. *Nat. Protoc.* 4:686–697.
46. Noguchi, H. 2013. Structure formation in binary mixtures of lipids and detergents: self-assembly and vesicle division. *J. Chem. Phys.* 138:024907.
47. Pizzirusso, A., A. De Nicola, ..., G. Milano. 2017. Biomembrane solubilization mechanism by Triton X-100: a computational study of the three stage model. *Phys. Chem. Chem. Phys.* 19:29780–29794.
48. Calvez, P., J. Jouhet, ..., A. Zapun. 2019. Lipid phases and cell geometry during the cell cycle of *Streptococcus pneumoniae*. *Front. Microbiol.* 10:351.
49. Marie, E., S. Sagan, ..., C. Tribet. 2014. Amphiphilic macromolecules on cell membranes: from protective layers to controlled permeabilization. *J. Membr. Biol.* 247:861–881.
50. Zylberberg, C., and S. Matosevic. 2016. Pharmaceutical liposomal drug delivery: a review of new delivery systems and a look at the regulatory landscape. *Drug Deliv.* 23:3319–3329.